https://doi.org/10.5194/egusphere-2026-4810
Preprint. Discussion started: 14 August 2026

Oleamide as a novel insoluble organic marker for reconstructing Arctic wildfire history in the ice core from southeastern Greenland

Mizuki Hirano[1,2*], Yoshinori Iizuka[2*], Takuto Ando[3], Kaoru Kawakami[2], Mai Matsumoto[1,2], Yutaka Kurosaki[2], Hiroshi Ohno[4], Sumito Matoba[2], Shoichi Mori[2], Yosuke Satoh[2], Fumiaki Saito[2]

[1] Graduate School of Environmental Science, Hokkaido University, Sapporo, 0600810, Japan
[2] Institute of Low Temperature Science, Hokkaido University, Sapporo, 0600819, Japan
[3] Graduate School of International Resource Sciences, Akita University, Akita, 0108502, Japan
[4] Kitami Institute of Technology, Kitami, 0908507, Japan

Correspondence to: Mizuki Hirano (hirano.mizuki.xg@gmail.com) and Yoshinori Iizuka (iizuka@lowtem.hokudai.ac.jp)

Present address: (Mizuki Hirano) Data Analytics Labo Co., Tokyo, Japan, and (Kaoru Kawakami) Tokyo Metropolitan Research Institute for Environmental Protection, Tokyo, Japan

Abstract. Global warming has intensified boreal forest fires, which significantly influence the climate through the emission of greenhouse gases and organic aerosols (OA). While water-soluble tracers are commonly used to reconstruct past fire events in ice cores, they can be susceptible to redistribution or degradation within the ice matrix. In this study, we performed single particle analysis of non-volatile microparticles in the SE-Dome II ice core from southeastern Greenland (1799–2020) using micro-Raman spectroscopy and Fourier-transform infrared spectroscopy (FT-IR). Here, we report the first identification of oleamide, an insoluble fatty acid amide, within an ice core. Oleamide is likely formed through the dehydration condensation of plant-derived oleic acid and ammonia under high-temperature (300-500 °C) conditions during forest fires. The detection frequency of oleamide particles was notably higher in layers corresponding to major North American forest fires, such as those in 1908, 1961, and 1994. Due to its insolubility and chemical stability, oleamide serves as a robust tracer that ensures stable long-range transport and long-term preservation in ice sheets. Additionally, cooling experiments revealed that oleamide possesses low ice-nucleating ability, likely due to the formation of expanded-phase monolayers. These results establish oleamide as a powerful new insoluble organic marker for reconstructing Arctic wildfire history and understanding historical fire-climate interactions.

1 Introduction

Global warming has intensified high-temperature and arid conditions, leading to the widespread expansion of forest fires (Sullivan et al., 2022). Between 2023 and 2024, the global forest disturbance area caused by fires reached 2.2 times the annual average recorded from 2002 to 2022 (Potapov et al., 2025). These fires not only disrupt ecosystems and accelerate species extinction but also serve as major sources of greenhouse gases and particulate matter that significantly influence the climate

https://doi.org/10.5194/egusphere-2026-4810
Preprint. Discussion started: 14 August 2026

(Sullivan et al., 2022; Zennaro et al., 2014; Legrand et al., 2016; Singh 2022). Organic aerosols (OA) are a primary component of fire-derived emissions; they act as ice nucleating particles, promoting cloud formation (Martins & Da Graca, 2018; Krishna et al., 2019; Parvin et al., 2019; Schiffman et al., 2025). Given that fire-derived OAs possess complex chemical structures and environmental impacts (Simoneit et al., 2002; Ditto et al., 2020), elucidating the morphology and chemical composition of fire-derived OA is essential.

More than 60% of the area burned between 2002 and 2024 occurred in boreal regions like Canada and Russia, representing a 2.3-fold increase over the past 24 years (Potapov et al., 2025). This trend is largely driven by climate change, with the Arctic warming at four times the global average (AMAP, 2021; Rantanen et al., 2022). Since boreal forests account for approximately 30% of global forest cover and terrestrial carbon storage (Zennaro et al., 2014), the expansion of fire activity in these regions could profoundly impact atmospheric CO_2 levels.

To evaluate long-term fire-climate interactions, data predating the satellite era (pre-1980s) are required. Ice cores are a powerful archive for such studies, as they preserve fire-derived aerosols (Zennaro et al., 2014; Legrand et al., 1992). In particular, high elevation sites in Greenland are ideally positioned to capture aerosol signals from boreal forest fires. While NH_4^+, NO_3^- and organic acids are established biomass burning indicators, specific tracers such as vanillic acid, levoglucosan, and dehydroabietic acid provide higher source specificity (Zennaro et al., 2014; Legrand et al., 1992, 2016; Parvin et al., 2019). These tracers, derived from the combustion of lignin, cellulose, and resins, are superior to multi-origin ions because they primarily originate from high-temperature plant combustion (Simoneit et al., 2002; Kutzer et al., 2024).

The Southeastern Dome (SE-Dome) region in Greenland is characterized by an exceptionally high snow accumulation rate (ca. 1 m water equivalent per year), which facilitates the preservation of chemical species such as NO_3^- that are otherwise prone to redistribution (Furukawa et al., 2017; Kawakami et al., 2023; Iizuka et al., 2025). Previous research at SE-Dome has successfully reconstructed Canadian fire histories over the past 60 years (Parvin et al., 2019). However, standard ions and water-soluble tracers such as levoglucosan may still be susceptible to redistribution or degradation within the ice matrix. In contrast, insoluble particles are hypothesized to be more stable, offering a robust record for reconstructing distant or small-scale fire events. Therefore, the objective of this study is to reconstruct the morphology and chemical composition of fire-derived particulate OA. We employed Raman spectroscopy and Fourier-transform infrared spectroscopy (FT-IR) to analyze non-volatile microparticles within the forest fire event layers of the SE-Dome II ice core, leading to the first identification of oleamide as a stable wildfire tracer.

2 Methods

2.1 The SE-Dome Ice Core and Forest Fire Event Identification

The SE-Dome II ice core was drilled between May and June 2021 in the SE-Dome region of southeastern Greenland (67°19′ 17″ N, 36°47′ 03″ W; 3,161 m a.s.l.; Iizuka et al., 2021). The 250-m core allows for paleoenvironmental reconstruction, such as past aerosol variations, from 1799 to 2020 (Kawakami et al., 2023; Iizuka et al., 2025). Because the high annual

https://doi.org/10.5194/egusphere-2026-4810
Preprint. Discussion started: 14 August 2026

accumulation rate of 1.02 m w.e. yr^{-1}, and the average accumulation is nearly constant throughout the year (Furukawa et al., 2017), the seasonal-scale reconstruction without seasonal accumulation bias is enables. In this study, forest fire events were identified based on peaks in NH_4^+ and NO_3^- concentrations (Figure A1; Iizuka et al., 2025), which were used to select samples for single particle analysis.

2.2 Extraction of Non-volatile Particles by Sublimation Method

Non-volatile microparticles were extracted using a sublimation method (Iizuka et al., 2009, 2012). To eliminate potential contamination, the surface layer of the ice core was removed using a pre-cleaned ceramic knife inside a class 100 clean booth located within a cold room (class 10,000; −22 °C). The cleaned ice sample was then shaved into a fine powder, and approximately 1 g of this powder was transferred onto an aluminum-foil-covered, circular stainless-steel plate (1 cm in diameter). For particle extraction, dry nitrogen gas was introduced through a metal pipe containing the sample inside an ultra-low-temperature freezer maintained at −50 °C, facilitating the complete sublimation of volatile matrix components, including ice. The remaining samples were immediately placed in a pre-cleaned stainless-steel Petri dish, which was sealed inside an ultra-clean polyethylene bag and stored in a desiccator at room temperature to prevent deliquescence.

2.3 Chemical Identification by Raman Spectroscopy

A total of 15 aluminum foil samples were prepared from core depths and time periods corresponding to the forest fire events listed in Table A1. Optical microscopic observation revealed dark (black/brown) and light-colored (white/translucent) particles with diameters exceeding approximately 1 μm. Raman spectra were acquired for an average of 67 particles per sample (totaling 1,139 particles across all 15 samples) using a micro-Raman spectrometer (XploRA LabSpec6, HORIBA). For comparative analysis, reference Raman spectra were also obtained for 63 reagent compounds.

Measurements were conducted at room temperature (ca. 25 °C) using either a 532-nm or 785-nm excitation laser. The specific analytical parameters were as follows: (1) gratings of 1800 grooves mm^{-1} and/or 1200 grooves mm^{-1}; (2) Raman shift ranges of 1800–4000 cm^{-1} (for the 532-nm laser) and 1200–2700 cm^{-1} (for the 785-nm laser); (3) an exposure time of 5 or 10 seconds per scan with 2 accumulations; and (4) wavenumber calibration using a standard silicon wafer (520 cm^{-1}). To prevent particle deliquescence during analysis, the microscope stage was continuously purged with dry air.

To evaluate potential procedural background contamination, frozen ultrapure water was processed using the exact same sublimation procedure; no particulate matter was detected on the resulting aluminum foil. Furthermore, reference Raman spectra of all experimental contact and packaging materials—including the aluminum foil, stainless-steel Petri dishes, and polyethylene bags—were confirmed to be distinct from any of the particle spectra reported in this study.

https://doi.org/10.5194/egusphere-2026-4810
Preprint. Discussion started: 14 August 2026

2.4 Elemental Analysis by SEM-EDS

Following the Raman analysis, particles exhibiting unique spectra—which had not been previously reported in ice-core microparticles and were suspected to consist of organic matter—were categorized from the 1908 and 1911 forest fire layers. To determine their elemental composition, six particles from the 1908 sample and 22 particles from the 1911 sample were analyzed using a scanning electron microscope (FlexSEM 1000II, HITACHI) equipped with an energy-dispersive X-ray spectrometer (AztecLive, OXFORD). Particles were located via secondary electron imaging and analyzed at an accelerating voltage of 20 keV with an acquisition time of 90 seconds.

Blank analyses performed at more than 30 random points on the aluminum foil substrate revealed that elements other than Al were rarely detected. Even when present, the peak intensities of these background elements remained within three standard deviations (3 σ) of the baseline noise. Consequently, for the ice-core particle analysis, elements other than Al were considered significantly present only when their peak intensities exceeded this 3 σ threshold.

2.5 Chemical characterization by FT-IR Spectroscopy

To validate the characterization of the unidentified organic particles tentatively classified by Raman spectroscopy, Fourier-transform infrared (FT-IR) microscopic analysis was performed using a Nicolet iN10 infrared microscope (Thermo Fisher Scientific). Spectra were acquired for the particles from the 1804 layer, including those exhibiting the unidentified Raman spectra, as well as for several reference standards: dehydroabietic acid, abietic acid, betulinic acid, and oleanolic acid. Measurements were conducted at a spatial resolution of several tens of micrometers over a wavenumber range of 650–4000 cm^{-1}. The attenuated total reflection (ATR) mode was employed using a germanium crystal (iN10 Ge Tip ATR) in contact with the sample, whereas atmospheric background spectra were collected with the crystal raised.

2.6 Ice-nucleating ability of ice-core samples

The ice-nucleating (IN) ability of the ice-core samples was evaluated using a custom-built cold-stage apparatus coupled with an optical microscope (e.g., Tobo et al., 2016). The system comprised a cooling chamber mounted on a stereomicroscope (BX-2700TL, WRAYMER), which was equipped with a high-resolution USB digital camera (NOA series, WRAYMER) to monitor the droplet freezing process in real-time.

Precise temperature regulation was achieved using a digital programmable controller (KP1000, CHINO Corporation) to manage the flow of liquid nitrogen to the cold stage. This setup maintained a constant cooling rate of 1.0 °C min^{-1} over a temperature range from +25 °C to −40 °C. To prevent the condensation of ambient moisture and subsequent frost formation on the sample surface, the interior of the cooling chamber was continuously purged with dry nitrogen gas provided by a dedicated generator. A melted droplet from the ice-core samples was positioned on the cold stage, and freezing events were recorded via time-lapse imaging at 2-second intervals with simultaneous temperature monitoring. The freezing temperature of each droplet was determined by detecting sudden changes in optical brightness from the time-lapse images.

https://doi.org/10.5194/egusphere-2026-4810
Preprint. Discussion started: 14 August 2026

3 Results

Raman spectra were acquired for a total of 63 reference standards, comprising 18 inorganic and 45 organic compounds (Figure A2). The organic suite included several species recognized as biomass burning tracers, such as levoglucosan, dehydroabietic acid, and vanillic acid, as well as carbohydrates (e.g., cellulose) and fatty acid salts (e.g., sodium oleate). To minimize the potential artifacts of the sublimation-based particle extraction process, water-soluble standards (primarily inorganic) were prepared as 1 wt% aqueous solutions using ultrapure water. These solutions were deposited onto glass slides and sublimated at −20 °C prior to Raman measurements. The Raman spectra of the inorganic compounds were characterized by single, sharp, and intense primary peaks. In contrast, the organic compounds exhibited a series of smaller peaks between 1000 and 1300 cm^{-1} (attributed to C-H, C-C, C-O, and C-N bonds) along with a prominent primary peak near 3000 cm^{-1} corresponding to C–H stretching vibrations (including those of CH_2 and CH_3 groups).

Figure 1 presents representative Raman spectra of the microparticles identified within the SE-Dome II ice core. Based on previous ice-core Raman studies (Ohno et al., 2005, 2006; Kawakami et al., 2022; Stoll et al., 2023), silicate minerals and calcium carbonate were identified (Figures 1a and 1b). Comparison with the reference standards also confirmed the presence of sodium sulfate (Figure 1c). Furthermore, we detected four distinct types of non-volatile microparticles exhibiting Raman spectra previously unreported in ice-core research:

Unidentified Particle 1: White particles (average diameter: $9.94 \pm 9.11\ \mu m$) characterized by multiple peaks between 1000 and 1300 cm^{-1} and a primary peak at 2883 cm^{-1} (Figure 1d).

Unidentified Particle 2: Black particles ($5.40 \pm 6.26\ \mu m$) showing two broad, overlapping peaks at 1341 and 1575 cm^{-1} (Figure 1e).

Unidentified Particle 3: Black particles ($5.06 \pm 4.66\ \mu m$) featuring peaks at 1341 and 1575 cm^{-1}, with an additional peak at 2694 cm^{-1} (Figure 1f).

Unidentified Particle 4: Black particles ($2.67 \pm 1.15\ \mu m$) with peaks at 292 and 390 cm^{-1}, and a dominant peak at 732 cm^{-1} (Figure 1g).

Particles exhibiting no detectable Raman signals were also observed (Figure 1h). Because Raman analysis is generally challenging for particles smaller than 1 μm, the average diameter of the analyzed particles was on the order of several micrometers, although numerous submicron particles were microscopically observed on the aluminum foils.

The temporal variations in the relative abundance of these detected substances are shown in Figure 2. Markers at the top of the panel indicate years characterized by high concentrations of NH_4^+ (circles), high NO_3^- (triangles), or low concentrations of both (unmarked). While mineral particles were present in all analyzed years except 1908 and 1961, inorganic compounds and Unidentified Particle 3 were detected only in specific sample layers. Unidentified Particle 1 was observed in all analyzed years except 1830 and 1920, showing higher detection frequencies during years with high NH_4^+ and NO_3^- concentrations. Notably, in the 1961 layer, this particle type accounted for 19% of the total particles (11 out of 57 particles).

https://doi.org/10.5194/egusphere-2026-4810
Preprint. Discussion started: 14 August 2026

A positive trend was observed between the NH_4^+ concentration and the detection frequency of Unidentified Particle 1 ($R^2 = 0.26$, $p = 0.051$).

4 Discussion

4.1 Chemical characterization and identification of non-volatile particles 1–4

For Unidentified Particle 4, mineral dust was considered the primary candidate due to the presence of characteristic Raman peaks below 1000 cm^{-1} typically associated with mineral species (Griffith, 1974). Particle 4 exhibited a prominent peak at 730 cm^{-1} (Figure 1g), which aligns closely with the reference spectrum of muscovite obtained from the Raman, X-ray, and UV-Visible Fluorescence Database (RRUFF database; http://rruff.info). Consequently, Particle 4 was confirmed to be muscovite, a silicate mineral.

To elucidate the chemical composition of Unidentified Particles 2 and 3, we compared their Raman spectra with those of common biomass burning (BB) tracers (vanillic acid, dehydroabietic acid, and levoglucosan), pyrogenic materials such as black carbon (BC), and various biogenic organic particles (pinonic acid, D-pinitol, betulinic acid, and cellulose). The Raman spectrum of Unidentified Particle 2 exhibited distinct, broad D and G bands at 1341 and 1575 cm^{-1}, respectively (Figure 1e). These features are consistent with the characteristic Raman signatures of BC (typically centered around 1360 and 1580 cm^{-1}) reported in previous studies, including soot particles derived from maize straw combustion (Sadezky et al., 2005; Pawlyta et al., 2015; Feng et al., 2019). Accordingly, Unidentified Particle 2 was identified as black carbon. Unidentified Particle 3 exhibited sharp peaks at 1346, 1579, and 2694 cm^{-1} (Figure 1f). These peaks matched the diagnostic D, G, and 2D bands of standard graphite reagents (typically observed near 1360, 1585, and 2700 cm^{-1}, respectively; Sze et al., 2001). Based on this spectral agreement, Particle 3 was classified as graphite.

Unidentified Particle 1 (Figure 1d) exhibited a cluster of peaks between 1000 and 1300 cm^{-1} (attributed to C–H, C–C, C–O, and C–N bonds) and a prominent primary peak at 2883 cm^{-1} (attributed to C–H, CH_2, and CH_3 stretching), characterizing it as an organic particle. Its frequent detection in samples with high NH_4^+ concentrations suggested a biomass burning (BB) origin. However, the Raman spectrum of Unidentified Particle 1 did not match any of the conventional BB tracers or biogenic organics tested (e.g., levoglucosan, pinitol, or cellulose; Figure S2). Elemental composition analysis of Unidentified Particle 1 (from the 1908 sample) via SEM-EDS revealed that carbon (C) and oxygen (O) were the primary constituents (Figure 3b), strongly supporting its classification as organic matter. Secondary electron (SE) imagery showed that these particles (approximately 5 μm in diameter) possessed an irregular, rounded morphology lacking sharp edges.

The FT-IR spectrum of Unidentified Particle 1 was compared with several organic standards commonly used as BB tracers, including oleanolic, betulinic, abietic, and dehydroabietic acids (Figure 4). Unidentified Particle 1 exhibited a primary

https://doi.org/10.5194/egusphere-2026-4810
Preprint. Discussion started: 14 August 2026

peak at 2920 cm^{-1} and additional peaks at 3394, 3186, 2850, 1647, 1632, 1470, and 1423 cm^{-1}. While all of these acid standards showed primary peaks in the 2928–2951 cm^{-1} range, their specific secondary peak patterns (such as the carbonyl bands at 1686–1697 cm^{-1}) differed substantially from those of Unidentified Particle 1. Consequently, the spectrum of Unidentified Particle 1 did not match any of the standard tracers shown in Figures 4c–4f. Instead, its main peaks at 2920 and 2850 cm^{-1} (C–H stretching) closely resembled the profile of oleic acid (Figure 4b), a ubiquitous vegetable-oil-derived fatty acid (Shults et al., 2023). Nevertheless, the presence of additional peaks at 3186 and 3394 cm^{-1}—indicative of N–H stretching (Coury and Dillner, 2008)—suggested that Unidentified Particle 1 was a nitrogen-containing derivative (specifically an amide) of oleic acid.

We subsequently evaluated three candidate compounds: ammonium oleate, sodium oleate, and oleamide. Based on physical properties, Unidentified Particle 1 was observed as a white solid, which effectively excluded ammonium oleate, as the latter typically exists as a viscous, yellow-brown liquid or paste. This identification was further confirmed through direct Raman and FT-IR comparisons. The Raman peak positions of Unidentified Particle 1 (with a primary peak at 2883 cm^{-1} and secondary peaks at 1649, 1443, 1295, 1118, 1061, and 873 cm^{-1}) were in excellent agreement with the oleamide reference standard (Figure 5e). Furthermore, the FT-IR peaks at 1427 (C–H bending), 1632 (C=O stretching), 2854 and 2928 (C–H stretching), and 3182 and 3360 cm^{-1} (N–H stretching) corroborated its identification as oleamide (Figure 5g). The absence of clear N–H bands in the spectra of ammonium oleate may stem from restricted molecular motion in its highly viscous state, which can also alter the fluorescence behavior of the sample during Raman analysis.

4.2 Formation process of oleamide particles

Raman and FT-IR spectroscopic analyses revealed, for the first time, the presence of oleamide particles within ice cores. The number of identified oleamide particles was elevated during years characterized by high concentrations of NO_3^- (1799, 1804, and 1877) and NH_4^+ (1908, 1911, 1940, 1961, 1970, 1992, 1994, and 2012) (Figure 2). Conversely, in years when no distinct peaks of ammonia or nitric acid were observed (1830, 1851, 1920, and 1989), the detection of oleamide (Unidentified Particle 1) was either zero or negligible (Figures 2 and A1). This close temporal correspondence suggests that oleamide particles originate from biomass burning (BB) events. A marginally significant positive correlation was observed between NH_4^+ concentrations and the detection counts of oleamide particles ($R^2 = 0.26$, $p = 0.051$). This modest correlation may be attributed to two main factors: first, NH_4^+ originates from diverse sources beyond forest fires, including agricultural and anthropogenic emissions (Iizuka et al., 2018); second, the particle counts obtained via Raman analysis are influenced by particle size and may be biased toward structurally ordered particles. Furthermore, because the Raman spectroscopic data are represented as particle counts, they limit direct quantitative comparison with mass concentrations. Nevertheless, this positive correlation suggests that both NH_4^+ and oleamide particles are influenced by shared source processes, such as major forest fires.

https://doi.org/10.5194/egusphere-2026-4810
Preprint. Discussion started: 14 August 2026

Notably, oleamide accounted for a high proportion of the total analyzed particles in the 1908, 1961, and 1994 layers, representing 16% (28 out of 178 particles), 19% (11 out of 57 particles), and 15% (8 out of 56 particles), respectively (Figure 2). Previous Greenland ice-core studies have confirmed that these specific years coincide with major wildfire activity, primarily in North America, as evidenced by elevated NH_4^+ concentrations and other established BB tracers (Legrand et al., 2016; Parvin et al., 2019).

The formation mechanism of oleamide and its utility as a forest fire proxy are discussed below. Oleamide is an organic compound containing an amide linkage (–CONH–), which is typically formed via the dehydration condensation of a carboxylic acid and ammonia. Oleic acid is a natural fatty acid abundant in plant lipids (Ma et al., 2024). The high-temperature environment generated during forest fires facilitates the volatilization and release of ammonia, which subsequently reacts with carboxylic acids, such as oleic acid, to yield amides (Simoneit et al., 2003; Ditto et al., 2022; Ma et al., 2024). Oleamide formation requires temperatures exceeding 300 °C, peaking at approximately 500 °C (Leng et al., 2020). At temperatures above 500 °C, further dehydration converts the amide group into a nitrile group, resulting in the formation of oleonitrile (Leng et al., 2020). Because temperatures exceeding 300 °C are highly unlikely to occur during atmospheric transport or after deposition on the ice sheet, oleamide is considered a primary thermal product formed by the reaction of plant-derived oleic acid and ammonia under the extreme heat of forest fires. Its secondary formation during transport or within the ice matrix is highly improbable.

Furthermore, fatty acid amides such as oleamide are chemically neutral, stable compounds characterized by extremely low water solubility (Oguro & Tsutsumi, 1966). Their resistance to atmospheric moisture facilitates stable long-range transport, and their low reactivity within the ice matrix ensures long-term preservation after deposition. Consequently, oleamide is more resistant to post-depositional degradation than water-soluble tracers such as levoglucosan. Because it exists in a stable particulate phase, oleamide serves as a robust wildfire tracer in ice cores. While historical wildfire reconstructions have traditionally focused on water-soluble species due to analytical convenience, insoluble fatty acid amides have been largely overlooked. This study demonstrates the efficacy of oleamide as a powerful and novel tracer for biomass burning.

As noted in the Introduction, the Arctic is warming at an accelerated rate; notably, over 60% of the global burned area between 2002 and 2024 occurred in boreal regions, such as Canada and Russia (AMAP, 2021; Rantanen et al., 2022; Potapov et al., 2025). Therefore, fire-derived organic aerosols, such as oleamide, are highly likely to be transported to and preserved in the Greenland ice sheet. While conventional tracers like levoglucosan and dehydroabietic acid are emitted during the combustion of specific vegetation types and may only occur in trace amounts as discrete particles, oleic acid is a major fatty acid ubiquitous across a wide range of plant species. This ubiquity suggests that substantial quantities of oleamide can be produced during intense wildfires, making it highly prevalent as a particulate marker in ice cores. The primary contribution of this study lies in the spectroscopic demonstration that oleamide persists in ice cores as solid-phase particles, thereby

https://doi.org/10.5194/egusphere-2026-4810
Preprint. Discussion started: 14 August 2026

establishing its efficacy as a novel proxy for reconstructing historical Arctic wildfires. Although the current methodology was limited to semi-quantitative spectroscopic analysis, future research should prioritize the development of chromatographic separation techniques to enable the precise quantification and interpretation of oleamide concentrations within ice-core records.

4.3 Ice-nucleating ability of oleamide

Previous research suggests that organic aerosol particles emitted during biomass burning events can function as ice-nucleating particles (INPs) (Schiffman et al., 2025). Accordingly, this study evaluated the ice-nucleating ability (INA) of the detected oleamide particles (see Section 2.6). We investigated two distinct freezing modes—immersion freezing and contact freezing—following the conceptual framework of Schiffman et al. (2025). For the immersion freezing assays, an aqueous suspension containing 1 wt% of the organic analyte was prepared. A 10 µL droplet of this suspension was placed onto a cartridge-type cooling substrate within the chamber to measure its freezing temperature. For the contact freezing assays, a single 2 µL droplet of ultrapure water was deposited onto a glass slide on the cooling substrate, and the freezing temperature was measured upon bringing the standard reagent particles into contact with the droplet interface. Ultrapure water and potassium feldspar (K-feldspar) were utilized as reference standards.

Table 1 presents the results of the droplet freezing experiments conducted on: (1) ultrapure water (blank reference), (2) K-feldspar (high-efficiency INP reference), (3) stearic acid reagent (a representative fatty acid), and (4) oleamide reagent. In the immersion freezing experiments, the mean freezing temperatures were recorded as −19.6 ± 0.8 °C (n = 10) for ultrapure water, −5.6 ± 1.2 °C (n = 5) for K-feldspar, −13.1 ± 1.2 °C (n = 5) for stearic acid, and −19.9 ± 1.5 °C (n = 5) for oleamide. Compared to ultrapure water, K-feldspar and stearic acid exhibited significantly higher freezing temperatures (by 14.0 °C and 6.5 °C, respectively), confirming their high INA. In contrast, the mean freezing temperature of oleamide was statistically indistinguishable from that of the ultrapure water blank.

In the contact freezing experiments, the mean freezing temperatures were −27.7 ± 2.3 °C (n = 5) for ultrapure water, −14.9 ± 1.1 °C (n = 5) for K-feldspar, and −26.2 ± 2.5 °C (n = 5) for oleamide. While K-feldspar maintained a high INA in this mode, the freezing temperature of oleamide remained within the experimental uncertainty of ultrapure water, showing no significant ice-nucleating activity.

Schiffman et al. (2025) suggested that relatively large organic aerosol particles (e.g., C18 species) can act as effective ice nuclei. However, DeMott et al. (2018) argued that long-chain fatty acids (C16 and C18) generally exhibit low INA due to their tendency to form monolayers. In the present study, stearic acid (a C18 fatty acid) showed a mean immersion freezing temperature of −13.1 ± 1.2 °C, which was notably higher than that of ultrapure water. It has been reported that INA depends strongly on structural compatibility with the ice lattice and the structural fluctuations of surface molecules (Qiu et al., 2017). Specifically, the formation of a highly ordered, condensed-phase monolayer with high surface pressure, which aligns effectively with the ice lattice, is suggested to promote ice nucleation (DeMott et al., 2018). Therefore, the elevated freezing temperature of stearic acid likely stems from the formation of such a stable, condensed-phase monolayer at the water droplet interface. Conversely, the immersion and contact freezing temperatures for oleamide (−19.9 ± 1.5 °C and −26.2 ± 2.5 °C,

https://doi.org/10.5194/egusphere-2026-4810
Preprint. Discussion started: 14 August 2026

respectively) were nearly identical to those of ultrapure water. Although oleamide is a fatty acid amide known to form monolayers (Miyashita et al., 2007), its low INA is likely attributable to the formation of an expanded-phase monolayer with low surface pressure in aqueous environments.

The contrasting behaviors of stearic acid and oleamide can be explained by their respective hydrophilic headgroups. Stearic acid is an amphiphilic molecule possessing a hydrophilic carboxyl group (COOH) and a hydrophobic alkyl chain (Moehwald et al., 2016; DeMott et al., 2018). The COOH group acts as a strong hydrogen-bond donor (Berlin et al., 2024), and the delicate balance between carboxyl hydration and hydrocarbon chain-chain interactions facilitates the formation of a tightly packed, high-surface-pressure condensed layer (Muro et al., 2010). In contrast, while oleamide possesses a hydrophilic amide group (CONH), nitrogen is less electronegative than oxygen, making the N–H bond a weaker hydrogen-bond donor than the O–H bond (Berlin et al., 2024). This implies that the intermolecular hydrogen-bonding network of the amide groups is weaker than that of the carboxyl groups in an aqueous environment. Consequently, fatty acid amide monolayers are more prone to lateral expansion and less likely to assemble into the highly ordered, crystalline-like structures characteristic of fatty acids. These findings lead to the conclusion that fatty acid amides, including oleamide, are unlikely to function effectively as ice-nucleating particles in the atmosphere.

4.4 Limitation of this study and future work

While this study successfully identified and characterized solid-phase oleamide particles in ice cores for the first time, several methodological and conceptual limitations remain to be addressed.

First, the spatial resolution of our micro-spectroscopic techniques (1-10 μm) inherently restricts detection to relatively large coarse-mode particles. Consequently, this approach potentially misses a significant fraction of submicron organic aerosols emitted during biomass burning (BB) events. Second, our current identification relies on discrete particle counts rather than continuous mass concentrations. This semi-quantitative nature likely accounts for the positive trend observed between oleamide particle counts and NH_4^+ concentrations ($R^2 = 0.26$, $p = 0.051$), as particle numbers do not directly translate to total aerosol mass fluxes. Third, although the structural ubiquity of the precursor oleic acid across various plant species enhances the detection probability of oleamide, it limits our ability to resolve source specificity, such as differentiating between specific fuel types (e.g., boreal forest conifers vs. agricultural residues). Finally, while our cooling assays demonstrated that oleamide exhibits negligible ice-nucleating ability (Section 4.3), its cloud condensation nuclei (CCN) activity and state of internal mixing with other atmospheric constituents remain unknown. These factors introduce uncertainties regarding its atmospheric lifetime and post-depositional scavenging efficiencies.

To overcome these limitations and fully establish oleamide as a robust wildfire proxy, future studies must transition to rigorous quantitative chemical analyses. Employing high-sensitivity chromatographic techniques, such as gas chromatography-mass spectrometry (GC-MS) or liquid chromatography-mass spectrometry (LC-MS), will enable the precise

https://doi.org/10.5194/egusphere-2026-4810
Preprint. Discussion started: 14 August 2026

quantification of bulk oleamide mass concentrations and fluxes within ice core records. Acquiring such quantitative, mass-based datasets is essential to establish robust statistical correlations with other multi-molecular fire tracers (e.g., levoglucosan and dehydroabietic acid) and to validate the application of oleamide for high-resolution reconstructions of long-term Arctic wildfire histories.

5 Conclusion

This study successfully characterized the morphology and chemical composition of fire-derived particulate organic aerosols (OAs) preserved in the SE-Dome II ice core from southeastern Greenland. Through individual particle analysis utilizing micro-Raman and Fourier-transform infrared (FT-IR) spectroscopies, we identified solid-phase oleamide particles within the ice core for the first time. Oleamide is an insoluble fatty acid amide formed via the dehydration condensation of plant-derived oleic acid and fire-emitted ammonia under the high-temperature conditions (300-500 °C) characteristic of intense forest fires. The detection frequency of these oleamide particles was notably elevated in ice layers characterized by high NO_3^- and NH_4^+ concentrations, closely coinciding with well-documented major North American wildfire events in 1908, 1961, and 1994. This temporal alignment demonstrates the efficacy of oleamide as a robust, insoluble proxy for historical biomass burning events. Unlike conventional water-soluble tracers such as levoglucosan, which are susceptible to post-depositional degradation or meltwater redistribution, oleamide exists as chemically neutral, stable solid particles with minimal water solubility. These intrinsic properties ensure stable long-range atmospheric transport and long-term preservation within the ice sheet matrix.

Furthermore, droplet freezing assays revealed that oleamide does not function as an effective ice-nucleating particle (INP) in either the immersion or contact freezing modes, exhibiting freezing temperatures that are statistically indistinguishable from those of ultrapure water. This negligible ice-nucleating ability is attributed to the formation of expanded-phase monolayers with low surface pressure at the aqueous interface, which lack the structural compatibility and packing density required to template ice lattice nucleation. Overall, the spectroscopic demonstration of solid-phase oleamide in ice cores establishes a novel framework for reconstructing past wildfire dynamics. Future integration of this particulate marker with high-sensitivity quantitative chromatography will further refine our understanding of long-term Arctic wildfire histories and their feedback within the rapidly changing polar climate system.

Figures and Tables

https://doi.org/10.5194/egusphere-2026-4810
Preprint. Discussion started: 14 August 2026

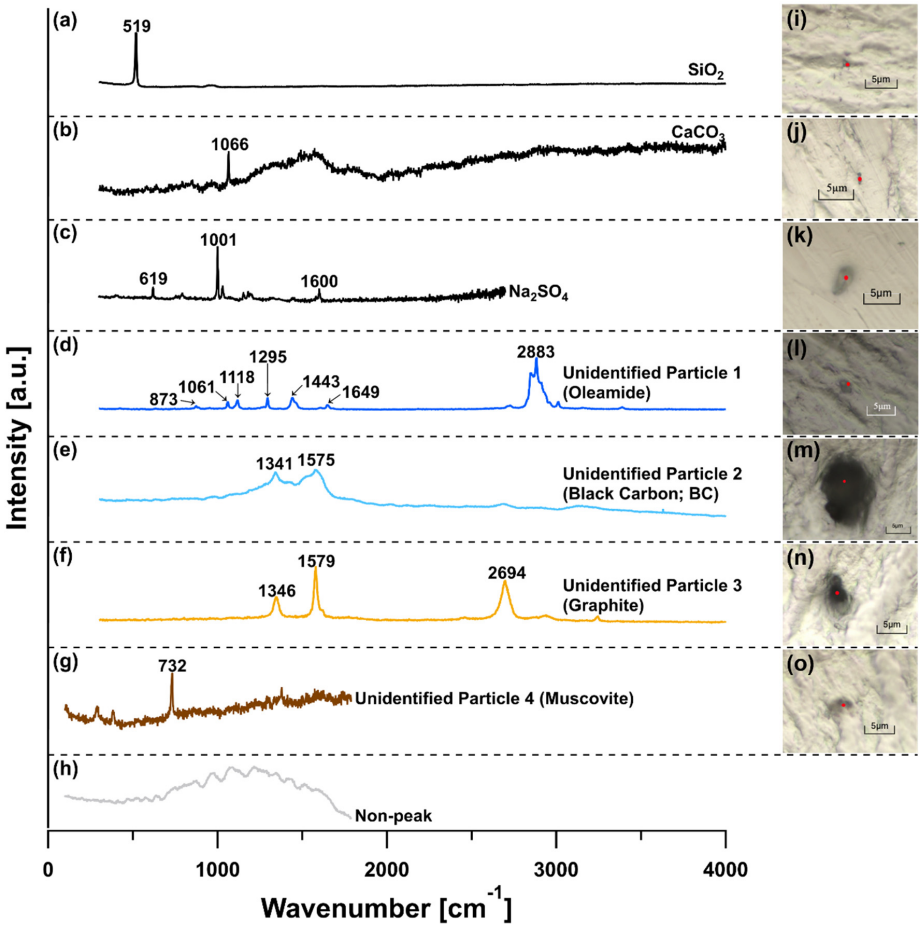

Figure 1: Representative Raman spectra and optical microscope images of non-volatile microparticles identified within the SE-Dome II ice core. The identified components include well-known inorganic species, such as (a) silicate minerals, (b) calcium carbonate, and (c) sodium sulfate, alongside four classes of initially unidentified microparticles evaluated in this study: (d) Unidentified Particle 1, (e) Unidentified Particle 2, (f) Unidentified Particle 3, and (g) Unidentified Particle 4. Panel (h) displays a representative spectrum exhibiting no detectable Raman signal. The microscope images in panels (i)–(o) correspond to the Raman spectra presented in panels (a)–(g), respectively.

https://doi.org/10.5194/egusphere-2026-4810
Preprint. Discussion started: 14 August 2026

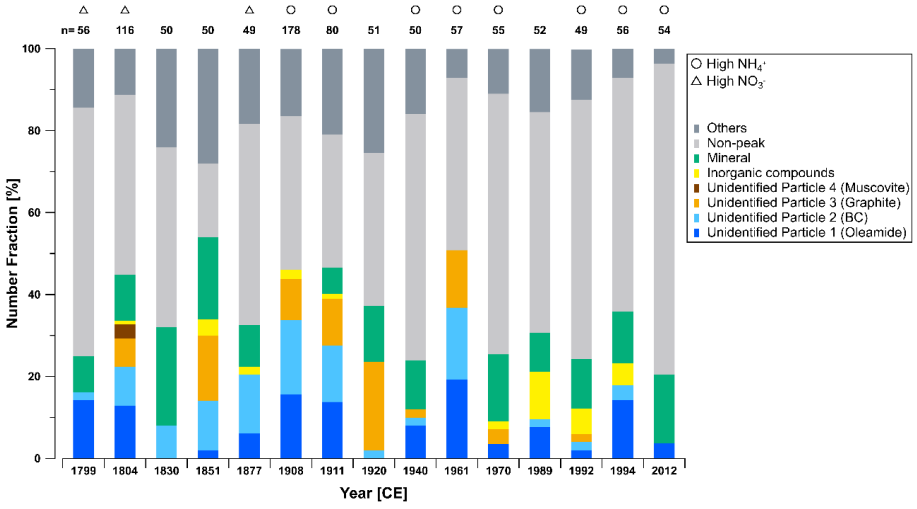

345 **Figure 2: Time series of the relative abundance of detected non-volatile microparticles in the SE-Dome II ice core. Markers at the top of the plot designate the sample categories: years with high NH_4^+ concentrations (circles), high NO_3^- concentrations (triangles), and low concentrations of both species (unmarked). The numbers below the markers indicate the total number of analyzed particles for each sample.**

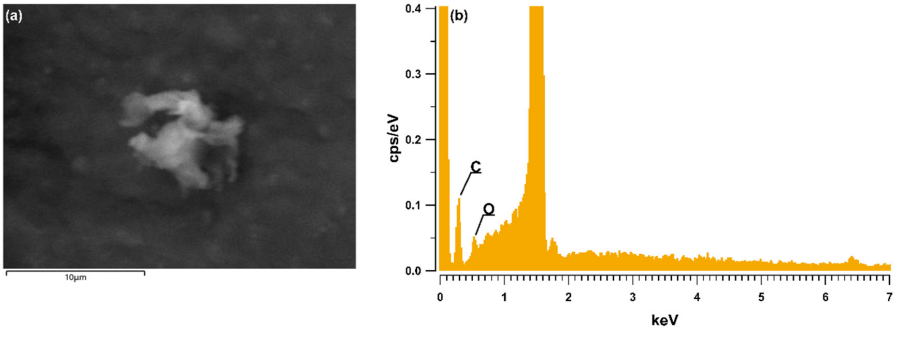

350 **Figure 3: Elemental composition analysis of Unidentified Particle 1 from the 1908 sample layer, obtained via Scanning Electron Microscopy with Energy Dispersive X-ray Spectroscopy (SEM-EDS). The spectrum reveals carbon (C) and oxygen (O) as the primary constituents. Note that the prominent peak at 1.49 keV corresponds to aluminum (Al) originating from the underlying aluminum foil substrate.**

355

https://doi.org/10.5194/egusphere-2026-4810
Preprint. Discussion started: 14 August 2026

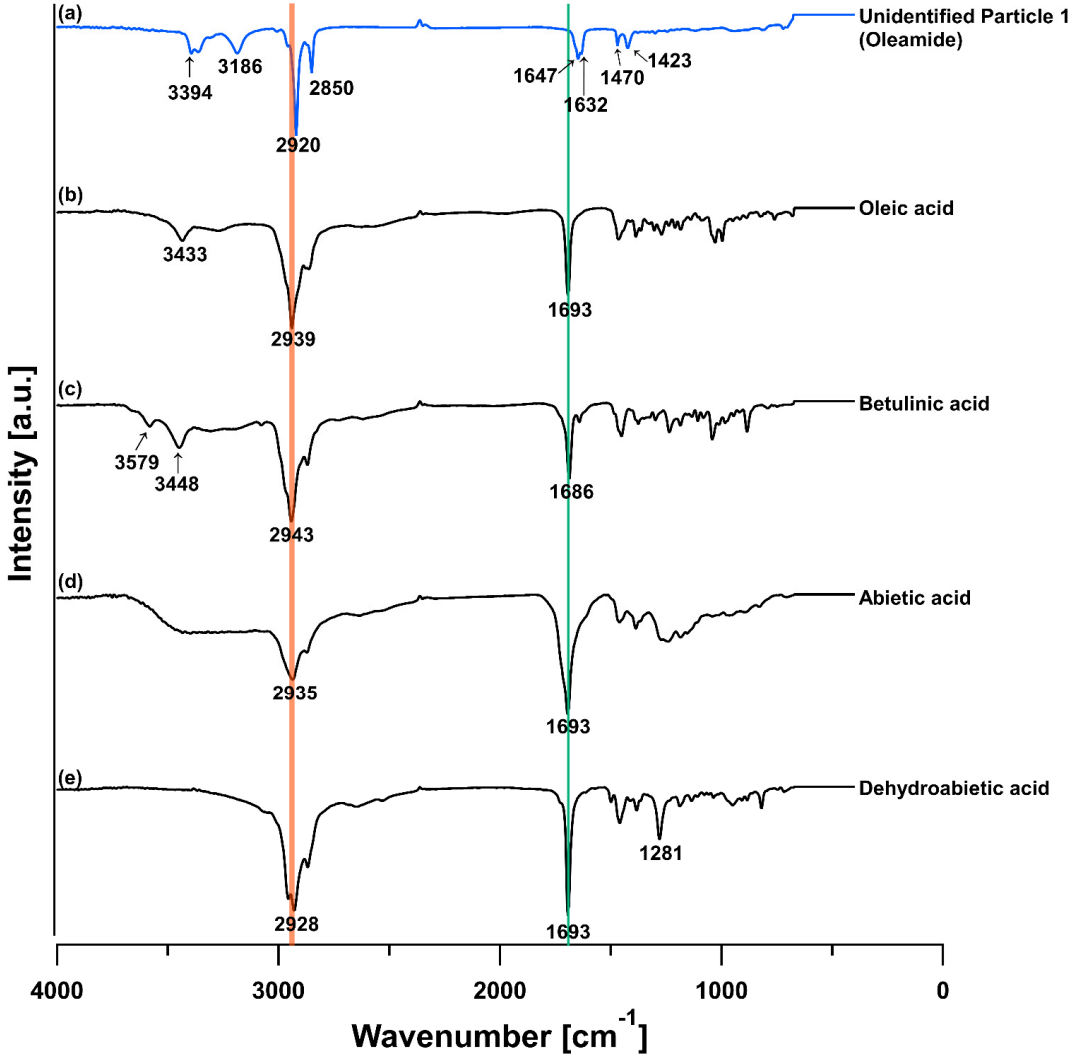

Figure 4: Comparison of the FT-IR spectrum of Unidentified Particle 1 (a) with those of several organic standards conventionally used as biomass burning tracers, including (b) oleic, (c) betulinic, (d) abietic, and (e) dehydroabietic acids. The red- and green-shaded regions correspond to the wavenumber ranges of 2928–2951 cm^{-1} and 1686–1697 cm^{-1}, respectively.

https://doi.org/10.5194/egusphere-2026-4810
Preprint. Discussion started: 14 August 2026

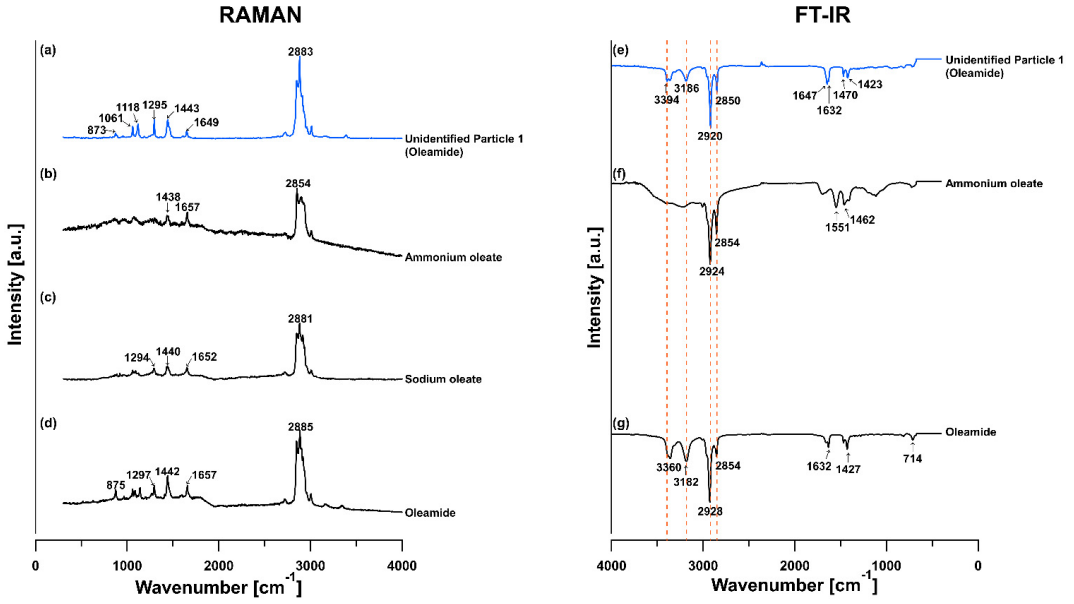

Figure 5: Comparison of Unidentified Particle 1 (a, e) with standard reagents of oleic salts (b–d, f, g) using Raman (left) and FT-IR (right) spectra. The close spectral agreement confirms the chemical identification of Unidentified Particle 1 as oleamide. The vertical red lines in the FT-IR panel (right) indicate the specific band positions at 2920, 2850, 3186, and 3394 cm^{-1}.

Table 1. Mean freezing temperatures of ultrapure water, K-feldspar, stearic acid, and oleamide determined via immersion (a) and contact (b) freezing experiments.

(a) Immersion freezing mode (1 wt% aqueous suspension)

Reagent	Chemical formulas	Mean freezing temperatures(°C)	Number of Measurements (n)
Ultra-pure water	H_2O	-19.6±0.8	10
K-feldspar	$KAlSi_3O_8$	-5.6±1.2	5
Stearic acid	$C_{18}H_{36}O_2$	-13.1±1.2	5
Oleamide	$C_{18}H_{35}NO$	-19.9±1.5	5

(b) Contact freezing mode

https://doi.org/10.5194/egusphere-2026-4810
Preprint. Discussion started: 14 August 2026

Reagent	Chemical formulas	Mean freezing temperatures(°C)	Number of Measurements (n)
Ultra-pure water	H_2O	-27.7±2.3	5
K-feldspar	$KAlSi_3O_8$	-14.9±1.1	5
Oleamide	$C_{18}H_{35}NO$	-26.2±2.5	5

375

Appendix A

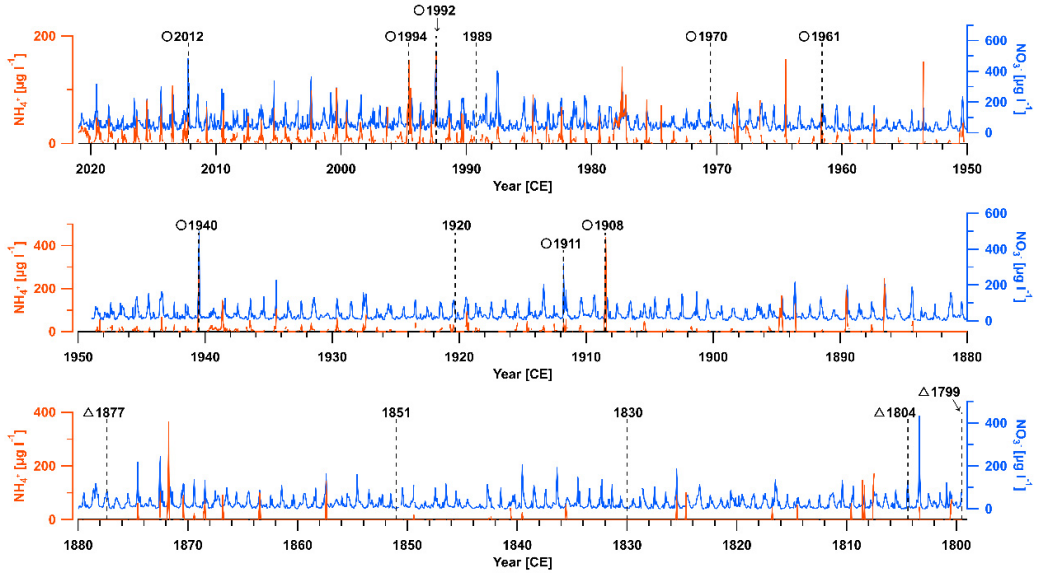

Figure A1: Temporal variations in NH_4^+ and NO_3^- concentrations in the SE-Dome II ice core. These ion profiles were utilized to reconstruct historical biomass burning events and to guide the selection of specific target layers for individual particle analysis.

380

https://doi.org/10.5194/egusphere-2026-4810
Preprint. Discussion started: 14 August 2026

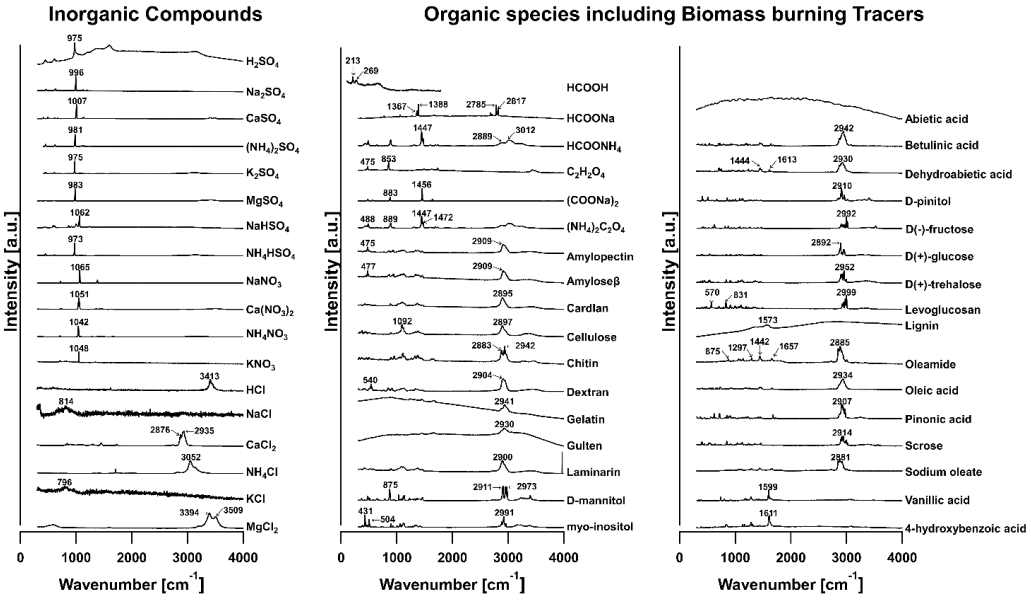

Figure A2: Reference Raman spectra obtained from 63 reference standards measured for comparison with the ice-core microparticles. The analyzed standards comprise 18 inorganic and 45 organic compounds, which are distributed across three panels: 385 **conventional organic biomass burning tracers (e.g., levoglucosan, dehydroabietic acid, and vanillic acid) in the right panel; other relevant organic species, including carbohydrates (e.g., cellulose) and fatty acid salts (e.g., sodium oleate) in the center panel; and inorganic compounds in the left panel.**

Table A1. Depths and corresponding chronological years of the 15 ice core samples analyzed in this study. The samples were selected 390 **based on periods associated with major biomass burning events.**

Depth [m]	Year [CE]	NH_4^+ [μg L^{-1}]	NO_3^-[μg L^{-1}]
249.91-250.45	1799.5-1800.0	n.a.	23.49
246.48-246.73	1804.2-1804.5	n.a.	98.21
221.82-222.70	1830.0-1831.0	n.a.	16.5
202.13-203.01	1851.0-1852.0	n.a.	18.52
177.30-177.93	1877.0-1878.0	n.a.	31.33
145.89-146.39	1908.3-1908.7	114.6	94.53

https://doi.org/10.5194/egusphere-2026-4810
Preprint. Discussion started: 14 August 2026

142.60-143.01	1911.6-1911.8	23.36	83.12
134.25-134.39	1920.3-1920.4	21.33	96.82
111.39-111.64	1940.4-1940.6	181.7	293.1
85.18-85.64	1961.6-1961.9	15.56	62.09
75.72-76.48	1970.3-1970.8	13.98	101.5
51.13-51.74	1989.1-1989.6	16	71.61
46.37-46.87	1992.3-1992.6	54.26	230.1
43.30-43.65	1994.3-1994.8	168.3	236.6
15.93-16.09	2012.1-2012.2	0.31	323.1

Data availability

The SE-Dome II ice core data used in this study are available from the Hokkaido University Collection of Scholarly and Academic Papers at https://doi.org/10.14943/2115.100156. The same dataset will also be archived in the Zenodo database before final publication.

Author contributions

Y.I. planned and supervised this study. M.H. and Y.I. contributed to the measurement of Raman and SEM-EDS data. M.H. and T.A. contributed to the FTIR data. M.H., Y.I., S.Mo, Y.S., and F.S. contributed to the measurement of the droplet freezing experiments. M.H. and Y.I. conducted data analyses. Y.I. wrote the original draft. M.H. and M.M. prepared the figures. M.H. and Y.I. wrote the manuscript. Y.I. acquired the funding. All the authors provided comments on the manuscript.

Competing interests

The authors declare that they have no conflict of interest.

Acknowledgements

The authors acknowledge the members of the SE-Dome Ice Core Project. Artificial intelligence support: Gemini was used to assist with English-language editing.

https://doi.org/10.5194/egusphere-2026-4810
Preprint. Discussion started: 14 August 2026

Financial support

This study was supported by MEXT/JSPS KAKENHI Grant Numbers (26K21778, 23H00511, and 24H00760), and the Arctic Challenge for Sustainability Project (Program Grant Number JPMXD1720251001).

References

AMAP, 2021. AMAP Assessment 2021: Impacts of Short-lived Climate Forcers on Arctic Climate, Air Quality, and Human Health. Arctic Monitoring and Assessment Programme (AMAP), Tromsø, Norway. x + 375pp

Arbiol, C. and Layne, G. D.: Raman Spectroscopy Coupled with Reflectance Spectroscopy as a Tool for the Characterization of Key Hydrothermal Alteration Minerals in Epithermal Au–Ag Systems: Utility and Implications for Mineral Exploration, Appl Spectrosc, 75, 1475–1496, https://doi.org/10.1177/00037028211047869, 2021.

Coury, C. and Dillner, A. M.: A method to quantify organic functional groups and inorganic compounds in ambient aerosols using attenuated total reflectance FTIR spectroscopy and multivariate chemometric techniques, Atmospheric Environment, 42, 5923–5932, https://doi.org/10.1016/j.atmosenv.2008.03.026, 2008.

Ditto, J. C., Joo, T., Slade, J. H., Shepson, P. B., Ng, N. L., and Gentner, D. R.: Nontargeted Tandem Mass Spectrometry Analysis Reveals Diversity and Variability in Aerosol Functional Groups across Multiple Sites, Seasons, and Times of Day, Environ. Sci. Technol. Lett., 7, 60–69, https://doi.org/10.1021/acs.estlett.9b00702, 2020.

Feng, Y., Liu, L., Yang, Y., Deng, Y., Li, K., Cheng, H., Dong, X., Li, W., and Zhang, L.: The application of Raman spectroscopy combined with multivariable analysis on source apportionment of atmospheric black carbon aerosols, Science of The Total Environment, 685, 189–196, https://doi.org/10.1016/j.scitotenv.2019.05.367, 2019.

Furukawa, R., Uemura, R., Fujita, K., Sjolte, J., Yoshimura, K., Matoba, S., and Iizuka, Y.: Seasonal-Scale Dating of a Shallow Ice Core From Greenland Using Oxygen Isotope Matching Between Data and Simulation, JGR Atmospheres, 122, https://doi.org/10.1002/2017JD026716, 2017.

Griffith, W. P.: Raman Spectroscopy of Minerals, in: The Infrared Spectra of Minerals, edited by: Farmer, V. C., Mineralogical Society of Great Britain and Ireland, Londan, 119–135, https://doi.org/10.1180/mono-4.8, 1974.

Iizuka, Y., Miyake, T., Hirabayashi, M., Suzuki, T., Matoba, S., Motoyama, H., Fujii, Y., and Hondoh, T.: Constituent elements of insoluble and non-volatile particles during the Last Glacial Maximum exhibited in the Dome Fuji (Antarctica) ice core, J. Glaciol., 55, 552–562, https://doi.org/10.3189/002214309788816696, 2009.

Iizuka, Y., Uemura, R., Motoyama, H., Suzuki, T., Miyake, T., Hirabayashi, M., and Hondoh, T.: Sulphate–climate coupling over the past 300,000 years in inland Antarctica, Nature, 490, 81–84, https://doi.org/10.1038/nature11359, 2012.

Iizuka, Y., Uemura, R., Fujita, K., Hattori, S., Seki, O., Miyamoto, C., Suzuki, T., Yoshida, N., Motoyama, H., and Matoba, S.: A 60 Year Record of Atmospheric Aerosol Depositions Preserved in a High-Accumulation Dome Ice Core, Southeast Greenland, JGR Atmospheres, 123, 574–589, https://doi.org/10.1002/2017JD026733, 2018.

https://doi.org/10.5194/egusphere-2026-4810
Preprint. Discussion started: 14 August 2026

Iizuka, Y., Matoba, S., Minowa, M., Yamasaki, T., Kawakami, K., Kakugo, A., Miyahara, M., Hashimoto, A., Niwano, M., Tanikawa, T., Fujita, K., and Aoki, T.: Ice Core Drilling and the Related Observations at SE-Dome site, southeastern Greenland Ice Sheet, Bulletin of Glacier Research, 39, 1–12, https://doi.org/10.5331/bgr.21R01, 2021.

Iizuka, Y., Matsumoto, M., Kawakami, K., Sasage, M., Ishino, S., Hattori, S., Uemura, R., Matsui, H., Fujita, K., Oshima, N., Spolaor, A., Svensson, A., Vinther, B. M., Ohno, H., Seki, O., and Matoba, S.: Acidity-driven gas-particle partitioning of nitrate regulates its transport to Arctic through the industrial era, Nat Commun, 16, 4272, https://doi.org/10.1038/s41467-025-59208-0, 2025.

Kawakami, K., Iizuka, Y., Matoba, S., Aoki, T., and Ando, T.: Inclusions in ice layers formed by melting and refreezing processes in a Greenland ice core, J. Glaciol., 69, 790–802, https://doi.org/10.1017/jog.2022.101, 2023a.

Kawakami, K., Iizuka, Y., Sasage, M., Matsumoto, M., Saito, T., Hori, A., Ishino, S., Fujita, S., Fujita, K., Takasugi, K., Hatakeyama, T., Hamamoto, S., Watari, A., Esashi, N., Otsuka, M., Uemura, R., Horiuchi, K., Minowa, M., Hattori, S., Aoki, T., Hirabayashi, M., Kawamura, K., and Matoba, S.: SE-Dome II Ice Core Dating With Half-Year Precision: Increasing Melting Events From 1799 to 2020 in Southeastern Greenland, JGR Atmospheres, 128, e2023JD038874, https://doi.org/10.1029/2023JD038874, 2023b.

Krishna, R. K., Panicker, A. S., Yusuf, A. M., and Ullah, B. G.: On the Contribution of Particulate Matter (PM2.5) to Direct Radiative Forcing over Two Urban Environments in India, Aerosol Air Qual. Res., 19, 399–410, https://doi.org/10.4209/aaqr.2018.04.0128, 2019.

Kutzer, K. and Meincken, M.: Retrospective determination of exposure temperature of standing trees during wildfires with solid-state NMR, Sci Rep, 14, 12821, https://doi.org/10.1038/s41598-024-63754-w, 2024.

Legrand, M., De Angelis, M., Staffelbach, T., Neftel, A., and Stauffer, B.: Large perturbations of ammonium and organic acids content in the summit-Greenland Ice Core. Fingerprint from forest fires?, Geophysical Research Letters, 19, 473–475, https://doi.org/10.1029/91GL03121, 1992.

Legrand, M., McConnell, J., Fischer, H., Wolff, E. W., Preunkert, S., Arienzo, M., Chellman, N., Leuenberger, D., Maselli, O., Place, P., Sigl, M., Schüpbach, S., and Flannigan, M.: Boreal fire records in Northern Hemisphere ice cores: a review, Clim. Past, 12, 2033–2059, https://doi.org/10.5194/cp-12-2033-2016, 2016.

Leng, L., Yang, L., Chen, J., Leng, S., Li, H., Li, H., Yuan, X., Zhou, W., and Huang, H.: A review on pyrolysis of protein-rich biomass: Nitrogen transformation, Bioresource Technology, 315, 123801, https://doi.org/10.1016/j.biortech.2020.123801, 2020.

Ma, Y.-J., Xu, Y., Yang, T., Xiao, H.-W., and Xiao, H.-Y.: Measurement report: Characteristics of nitrogen-containing organics in $PM_{2.5}$ in Urumqi, northwest China: differential impacts of combustion of fresh and old-age biomass materials, https://doi.org/10.5194/egusphere-2023-2514, 4 January 2024.

Martins, N. R. and Carrilho Da Graça, G.: Impact of PM2.5 in indoor urban environments: A review, Sustainable Cities and Society, 42, 259–275, https://doi.org/10.1016/j.scs.2018.07.011, 2018.

https://doi.org/10.5194/egusphere-2026-4810
Preprint. Discussion started: 14 August 2026

Oguro, M. and Tsutsui, Y.: The Properties and Application of Fatty Amides, J. Jpn. Oil. Chem. Soc., 15, 406–415, https://doi.org/10.5650/jos1956.15.406, 1966.

Ohno, H., Igarashi, M., and Hondoh, T.: Salt inclusions in polar ice core: Location and chemical form of water-soluble impurities, Earth and Planetary Science Letters, 232, 171–178, https://doi.org/10.1016/j.epsl.2005.01.001, 2005.

Ohno, H., Igarashi, M., and Hondoh, T.: Characteristics of salt inclusions in polar ice from Dome Fuji, East Antarctica, Geophysical Research Letters, 33, 2006GL025774, https://doi.org/10.1029/2006GL025774, 2006.

Parvin, F., Seki, O., Fujita, K., Iizuka, Y., Matoba, S., Ando, T., and Sawada, K.: Assessment for paleoclimatic utility of biomass burning tracers in SE-Dome ice core, Greenland, Atmospheric Environment, 196, 86–94, https://doi.org/10.1016/j.atmosenv.2018.10.012, 2019.

Pawlyta, M., Rouzaud, J.-N., and Duber, S.: Raman microspectroscopy characterization of carbon blacks: Spectral analysis and structural information, Carbon, 84, 479–490, https://doi.org/10.1016/j.carbon.2014.12.030, 2015.

Potapov, P., Tyukavina, A., Turubanova, S., Hansen, M. C., Giglio, L., Hernandez-Serna, A., Lima, A., Harris, N., and Stolle, F.: Unprecedentedly high global forest disturbance due to fire in 2023 and 2024, Proc. Natl. Acad. Sci. U.S.A., 122, e2505418122, https://doi.org/10.1073/pnas.2505418122, 2025.

Rantanen, M., Karpechko, A. Yu., Lipponen, A., Nordling, K., Hyvärinen, O., Ruosteenoja, K., Vihma, T., and Laaksonen, A.: The Arctic has warmed nearly four times faster than the globe since 1979, Commun Earth Environ, 3, 168, https://doi.org/10.1038/s43247-022-00498-3, 2022.

Sadezky, A., Muckenhuber, H., Grothe, H., Niessner, R., and Pöschl, U.: Raman microspectroscopy of soot and related carbonaceous materials: Spectral analysis and structural information, Carbon, 43, 1731–1742, https://doi.org/10.1016/j.carbon.2005.02.018, 2005.

Schiffman, Z. R., McMillan, K. A., Johnson, D. M., Gough, R. V., Davis, R. D., Brooks, S. D., and Tolbert, M. A.: Contact Freezing of Water Droplets by Crystalline Organic Acids, J. Phys. Chem. A, 129, 7482–7495, https://doi.org/10.1021/acs.jpca.5c03258, 2025.

Shults, A. A., Lu, G., Caldwell, J. D., and Macdonald, J. E.: Role of carboxylates in the phase determination of metal sulfide nanoparticles, Nanoscale Horiz., 8, 1386–1394, https://doi.org/10.1039/D3NH00227F, 2023.

Simoneit, B. R. T.: Biomass burning — a review of organic tracers for smoke from incomplete combustion, Applied Geochemistry, 17, 129–162, https://doi.org/10.1016/S0883-2927(01)00061-0, 2002.

Simoneit, B. R. T., Rushdi, A. I., Bin Abas, M. R., and Didyk, B. M.: Alkyl Amides and Nitriles as Novel Tracers for Biomass Burning, Environ. Sci. Technol., 37, 16–21, https://doi.org/10.1021/es020811y, 2003.

Singh, S.: "Forest fire emissions: A contribution to global climate change," Front. For. Glob. Change, 5, 925480, https://doi.org/10.3389/ffgc.2022.925480, 2022.

Stoll, N., Westhoff, J., Bohleber, P., Svensson, A., Dahl-Jensen, D., Barbante, C., and Weikusat, I.: Chemical and visual characterisation of EGRIP glacial ice and cloudy bands within, The Cryosphere, 17, 2021–2043, https://doi.org/10.5194/tc-17-2021-2023, 2023.

https://doi.org/10.5194/egusphere-2026-4810
Preprint. Discussion started: 14 August 2026

Sze, S.: Raman spectroscopic characterization of carbonaceous aerosols, Atmospheric Environment, 35, 561–568, https://doi.org/10.1016/S1352-2310(00)00325-3, 2001.

Tobo, Y.: An improved approach for measuring immersion freezing in large droplets over a wide temperature range, Sci Rep, 6, 32930, https://doi.org/10.1038/srep32930, 2016.

Zennaro, P., Kehrwald, N., McConnell, J. R., Schüpbach, S., Maselli, O. J., Marlon, J., Vallelonga, P., Leuenberger, D., Zangrando, R., Spolaor, A., Borrotti, M., Barbaro, E., Gambaro, A., and Barbante, C.: Fire in ice: two millennia of boreal forest fire history from the Greenland NEEM ice core, Clim. Past, 10, 1905–1924, https://doi.org/10.5194/cp-10-1905-2014, 2014.